Femtosecond Direct Laser Interference Patterning of Nickel Electrodes for Improving Electrochemical Properties

Fabian Ränke[1*], Stephan Moghtaderifard[1], Lis Zschach[1], Robert Baumann[1], Bogdan Voisiat[1], Marcos Soldera[1], Leonard Günther[1], Sebastian Hilbert[2], Christian Immanuel Bernäcker[2], Thomas Weißgärber[2], and Andrés Fabián Lasagni[1,3]

[1]*Institut für Fertigungstechnik, Technische Universität Dresden, Germany*
[2]*Fraunhofer Institute for Manufacturing Technology and Advanced Materials IFAM, Germany*
[3]*Fraunhofer-Institut für Werkstoff- und Strahltechnik IWS, Germany*
[*]*Corresponding author's e-mail: Fabian.raenke@tu-dresden.de*

The present work utilizes Direct Laser Interference Patterning (DLIP) to impart periodic microstructures onto the surface of nickel foils. A pulsed laser source emitting green radiation (514 nm) with pulse duration between 282 fs and 1 ps is utilized to produce line and cross-like pattern geometries having a spatial period of 3.0 µm and a maximum structure depth of ~ 2.8 µm. Both the pulse duration and number of consecutive scans are varied in order to assess their influence on the structure formation. Afterwards, the treated Ni- electrodes are used for alkaline water electrolysis. The most active electrode exhibits an overpotential of -227 mV at a current density of -0.5 A cm^{-2} for the Hydrogen Evolution Reaction (HER). Thus, the technique here proposed permitted a 51 % reduction in the overpotential of the HER compared to the untreated Ni-electrode, opening up possibilities for the development of more efficient electrodes for hydrogen production.

DOI: 10.2961/jlmn.2024.02.2002
Keywords: direct laser interference patterning, nickel electrodes, alkaline electrolysis, hydrogen evolution reaction

1. Introduction

Climate change represents an urgent and pressing challenge that demands immediate attention and concerted action. One crucial aspect of mitigating carbon emissions and facilitating a sustainable future lies in the adoption of hydrogen as a key energy carrier and storage medium [1]. Hydrogen possesses immense potential for energy recovery when utilized in fuel cells, as its combustion yields electrical energy, with water being the sole by-product. Among the various methods of large-scale hydrogen production, alkaline water electrolysis stands out as a particularly promising technique for meeting the growing demand for hydrogen in a sustainable manner, contributing to the transition to a low-carbon economy [2]. However, the efficiency and durability of alkaline water electrolysis systems rely heavily on the quality and performance of their electrodes. In case of the hydrogen evolution reaction (HER), it has been shown that the reaction efficiency can be enhanced by (i) increasing the real surface area and/or (ii) improving the intrinsic activity of the electrode materials, leading to a reduction of the overpotential ηHER [3–5]. In the hydrogen evolution reaction, the overpotential refers to the reaction rate and is directly proportional to the additional energy required to drive the reaction forward and is directly related to the efficiency of the HER, as it affects the rate at which hydrogen is produced [6,7]. Nickel and nickel alloys (e.g. Raney Ni, Ni-Mo) are common choices for this process due to their excellent electro catalytic activity and long-term stability [8–10]. In particular, it has been shown that the HER activity of these electrodes can benefit tremendously when the surface area is increased [9,11,12]. In recent years, laser texturing of nickel electrodes has emerged as an attractive manufacturing method to improve the efficiency of the electrode towards HER [3,6,13,14]. Generally, laser texturing of surfaces has many advantages over conventional methods, since they allow a precise control of the size, shape, and distribution of surface features [15,16]. In previous studies, complex surface architectures on metallic electrodes were produced with repetitive or quasi-periodic arrangements using laser-based methods. In this way, they have been implemented to significantly enlarge their surface area and thus improving their electrochemical activity. For example, Direct Laser Writing (DLW) was used to structure nickel electrodes for applications in electro-catalysis and energy storage [4,6,17]. In this context, Rauscher et al. employed a femtosecond pulsed laser to fabricate self-organized conical microstructures on nickel electrodes, resulting in a 45% enhancement of the HER efficiency [6]. However, when features with lateral sizes below a few microns are needed, DLW faces the limitations of a reduced throughput as well as resolutions restrictions imposed by the diffraction limit. One promising laser texturing method capable to overcome these challenges is Direct Laser Interference Patterning (DLIP) [18]. This method has been used to create a variety of surface structures, such as microchannels, micropillars, and microdimples, on various nickel alloys. The DLIP method is based on overlapping two or more coherent laser beams on the sample surface to produce an interference pattern with a periodic distribution of the laser intensity [19,20]. Subsequently, material ablation or melting predominantly takes place in areas corresponding to the interference maxima positions where the melting/ablation threshold fluence/s is/are surpassed. Conversely, areas subjected to destructive interference (interference minima positions) remain unaffected. In the context of alkaline water

electrolysis, laser texturing of nickel electrodes by DLIP has recently shown to significantly improve their performance due to the creation of microscale surface features that enlarge the surface area, generating active centres for hydrogen evolution. For example, Baumann et al. utilized DLIP with ps-pulses on open cell metal foams (steel 316L (1.4404)) [21]. In the mentioned work, the electrochemical performance of the textured foams revealed an increase of the double-layer capacitance from 702 µF cm^{-2} (unstructured material) to 1330 µF cm^{-2} for the DLIP treated foam, what was related to an enlargement of the electrochemical surface by a factor of almost two. However, the impact of implementing shorter pulses up in the femtosecond (fs) range on the efficiency of DLIP treatment for achieving higher performances remains unclear until now. This work explores the benefits of DLIP texturing of nickel electrodes using pulse durations in the fs range in order to improve their performance in the hydrogen evolution reaction. The structuring of the Ni-foils is performed with a laser source emitting green radiation (514 nm) with pulse durations of 282 fs, 1 ps and 10 ps, and varying the laser fluence and number of scans. The topography of the treated surfaces is characterized using confocal and scanning electron microscopy methods. Finally, the performance of the treated samples if characterized in an alkaline water electrolysis.

2. Experimental Section

2.1 Materials

For all laser structuring experiments, commercially available nickel sheets (99.95% purity, Goodfellow, USA) with a thickness of 125 µm and dimensions of 300 mm x 300 mm were used. Prior to laser processing, the samples were cleaned with ethanol (ethanol absolute ≥ 99.9 %, Supelco, Germany) to remove any possible contamination and subsequently dried with compressed air.

2.2 Laser texturing process

The laser structuring through DLIP was performed by using the optical configuration illustrated in Figure 1a. The fs-DLIP setup is equipped with a femtosecond solid-state laser (Carbide-40W-SH-TH, Light Conversion UAB, Lithuania) with a maximum pulse energy of 400 µJ. The laser operated at a wavelength ʎ of 514 ± 3 nm with a tunable pulse duration τ ranging from 282 fs to 10 ps and a repetition rate f_{rep} of 1 kHz. The beam path consisted of telescope system that acts as a beam expander, and a recently developed optical head for DLIP (xDLIP head, SurFunction GmbH, Germany) that utilizes a Diffractive Optical Element (DOE) to split the main laser beam into two sub-beams, which are later shaped to elongated lines (see Figure 1b) and overlapped on the sample. This optical configuration had the advantage over previous setups that can be used with shorter pulse durations (in the fs range) as well as an impressive depth of focus of ~ 10 mm [22]. The resulting focal spot had an elliptical shape with dimensions of (dy × dx) 0.1 mm × 2.5 mm (Figure 1b).

Using this optical configuration, an intercepting angle Θ between the overlapping beams of 9.8 ° is obtained. Considering this angle as well as the used laser wavelength ʎ, the spatial period of the interference pattern can be calculated by using equation (1):

$$\Lambda = \frac{\lambda}{2 \cdot \sin(\theta/2)}. \quad (1)$$

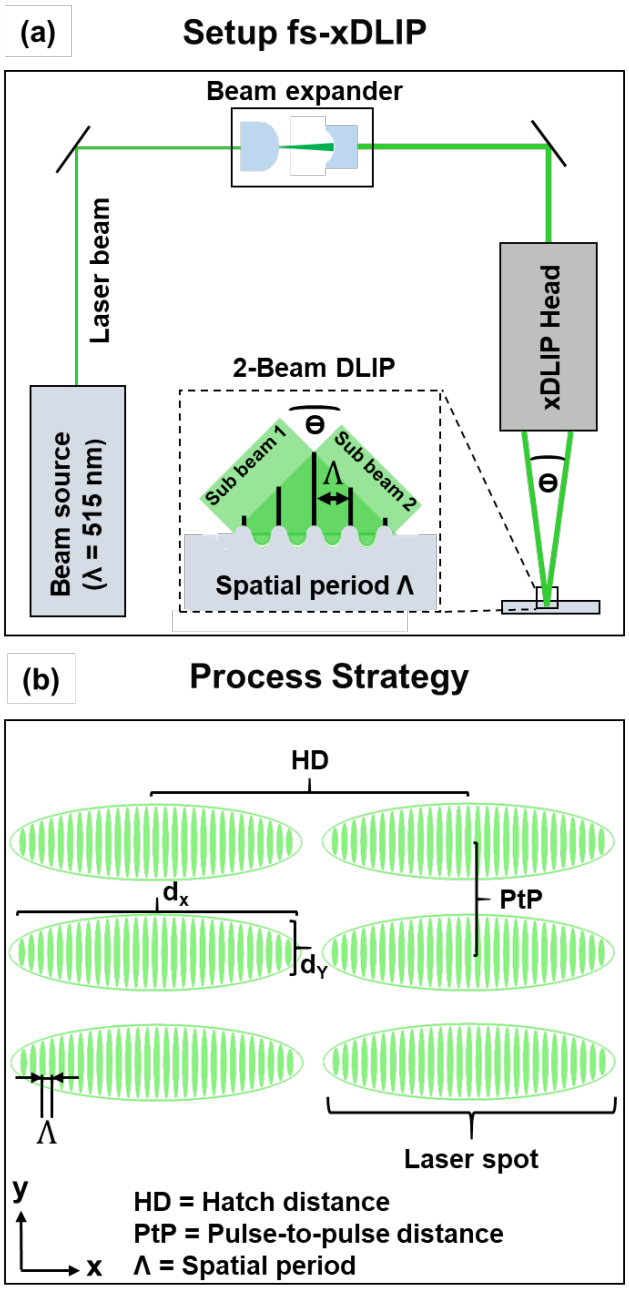

Fig. 1 (a) Schematic drawing of the used experimental setup showing the two-beam DLIP optical configuration combined with a xDLIP head.[22] The inset denotes the two overlapping sub-beams producing a line-like interference pattern. (b) Process strategy for structuring surfaces with elongated laser spots and corresponding process parameters.

As a result, the overlapped sub-beams produce an interference pattern, consisting of periodically distributed lines with a spatial period Λ of ~3.0 µm, which are oriented perpendicular to the long axis of the elliptical laser spot (Figure 1b). During the processing, the elongated laser spot was translated along the direction of the interference lines by moving the sample at different process speeds leading to various pulse-to-pulse distances PtP at a fixed repetition rate frep. The movement of the nickel foils in two-

dimensional directions was done with mechanical stages (Aerotech PRO155-05, USA). Considering the size of the laser spot in the y-direction (~ 100 µm, Figure 1b) and the used pulse-to-pulse distance PtP, then it is possible to calculate the overlap OV (in %) by using equation (2):

$$OV = (1 - \frac{\mathrm{PtP}}{d_y}) \cdot 100\% \cdot \quad (2)$$

For the fabrication of line-like surface patterns with different structure depths, the number of consecutive passes N (scans) was varied from 1 to 30 for a fixed pulse-to-pulse distance PtP of 5.5 µm (OV = 95 %). This resulted in different cumulated fluences (from 0.2 to 22.0 J cm^{-2}), which describes the total laser energy used to irradiated a specific area. For the treatment of large areas, the hatch distance HD, which is the lateral distance between pulses (Figure 1b), was set to 130 times the spatial period Λ, resulting in 390 µm. Additionally, to understand the influence of thermal effects on the resulting structure topography, the laser pulse duration τ was varied, using 282 fs, 800 fs and 1 ps pulses.

2.3 Topographical characterization

For evaluating the surface topography of the laser structured samples, confocal microscopy images (Sensofar S-Neox, Spain) were recorded by employing 50x and 150x magnification objectives. The surface profiles and average structure depth values were obtained using the SensoMAP Advanced Analysis Software (Sensofar, Spain). In addition, high resolution images of the treated Ni-samples were taken using Scanning Electron Microscopy (SEM) operating at an acceleration voltage of 30 kV (Quattro ESEM, Thermo Fischer Scientific, Germany). The resulting images were also evaluated with Gwyddion software by using the two-dimensional Fast Fourier transformation, permitting the determination of structural characteristics for fabricated surface structures.

2.4 Electrochemical characterization

The electrochemical characterization of the electrodes was conducted in a conventional three-electrode cell configuration at a temperature of 60 °C with 30 wt.-%. KOH. For the counter electrode a platinum sheet (8 cm²) was utilized, and a saturated Reversible Hydrogen Electrode (RHE) was used as the reference electrode. The separation of the electrodes was achieved by a Haber-Luggin. A two-chamber cell with a diaphragm (Zirfon Perl 500 UTP, Mortsel) was used to separate anolyte and catholyte. The temperature of the double-wall electrochemical cell was controlled by an external thermostat (ΔT = ± 2 K). The electrolyte solution was rinsed with gaseous nitrogen before the experiments. All current densities (j_{geo}) are referred to the geometric surface area of the electrodes (A_{geo} = 2 cm^2).

The Electrochemically active Surface Area (ECSA) of the electrodes was estimated by determination of the double-layer capacitance C_{dl}, using Electrochemical Impedance Spectroscopy (EIS) [23]. The EIS measurements were performed in a frequency range between 0.05 Hz and 15 kHz with an ac amplitude of 5 mV. The RandlesCPE fitting routine of the software "Gamry Echem Analyst" (Gamry Instruments) was used for data analysis. In addition, the dimensionless roughness factor R_f is calculated as the ratio between the double-layer capacitance C_{dl} of the laser structured electrodes and untreated Ni-electrode. The steady-state polarization curves were galvanostatically recorded in the range of j_{geo} = -0.001 to -0.5 Acm^{-2}; each step for 20 s in the direction of decreasing current density. Previously, the electrodes were polarized at a current density of -0.5 A cm^{-2} for 1 h, inducing the evolution of hydrogen gas.

3. Results and discussion

3.1 Influence of process parameter on the surface topography

Line-like DLIP textures with a spatial period Λ of ~3.0 µm were firstly fabricated on the Ni-foils. As process parameters, the pulse duration τ and number of consecutive passes N were varied to evaluate their influence on the structure morphology. As mentioned before, the repetition rate frep was kept constant for all experiments. In the course of the investigations performed, the pulse energy was gradually increased from 41.1 to 90.8 µJ. The total energy applied per unit of area, known as the cumulated laser fluence Φ_{cum}, was calculated using Equations (4) and (5),

$$N_{Pulses} = \frac{d_y \cdot f_{rep}}{v_{scan}}, \quad (4)$$

$$\Phi_{cum} = \frac{E_P}{A_{spot}} \cdot N_{pulses} \cdot N, \quad (5)$$

where $A_{spot} = \pi \times dx/2 \times dy/2$ is the laser spot area, and N_{pulses} the number of applied laser pulses irradiating the same effective area, that can be calculated from Equation (4). Figure 2 shows SEM images of selected patterned Ni-surfaces, where well-defined line-like textures can be observed. The used pulse durations were 1 ps for the SEM image shown in Figure 2a, d, 800 fs for Figure 2b, e, and finally 282 fs for Figure 2c, f. Moreover, the structures shown in images (a, b, c) were produced with a single scan, whereas the patterns in (d, e, f) were fabricated with 20 consecutive passes. In all samples, the overlap OV was kept constant at 95 % (see experimental section). The calculated cumulated fluences are given in the labels for each sub-figure.

For the samples structured with a single pass (N = 1) and different pulse durations, the appearance of a homogenous line-like DLIP pattern decorated with a sub-structure can be observed. Upon inspecting the samples structured with a pulse duration of 1 ps (Figure 2a) and 800 fs (Figure 2b) at a higher magnification (see insets), the presence of a wavy texture at the positions corresponding to the interference maxima can be observed. These ripples are oriented perpendicular to the polarization of the applied laser radiation (double arrow E in Figure 2a) and follow along the DLIP produced lines. The measured periodicity of the ripples ranged from 350 nm to 410 nm, which corresponds to 68% - 80% of the used laser wavelength (514 nm). These characteristics suggest that the sub-structure can be regarded as Laser-Induced Periodic Surface Structures (LIPSS)

and further classified as Low-Spatial Frequency LIPSS (LSFL), according to previous studies [24–26].

In the case of the texture shown in Figure 2c, produced with the shortest pulse duration of 282 fs, no visible ripples were found but instead a random sub-texture was produced. Also nanoparticles distributed over the whole area are visible. Taking into consideration matter reorganization theories, it is known that phase transitions as well as hydrodynamic effects of the transiently melted surface are necessary for LIPSS formation [27]. For instance, the existing theories are driven by local gradients and require the surface to stay long enough in an excited state that enables the underlying mechanisms to act. Hence, these effects dominate for long pulse durations and could explain why the LIPSS are only observed for the longer pulse durations (800 fs and 1 ps). An alternative perspective involves examining the correlation between threshold fluence and pulse duration, as both factors significantly influence the formation of LIPSS. Fundamentally, threshold fluences decrease with decreasing pulse durations. When maintaining a constant cumulative fluence while decreasing pulse durations, the formation conditions (typically close to the material's ablation threshold) for LIPSS structures shift into a range well above the established formation regime. Consequently, no self-organizing LIPSS textures are produced [27]. By increasing the number of consecutive passes (N) to 20, the cumulated laser fluence was increased from 0.7 to 14.5 J cm^{-2}. As a consequence, the ablation at the maxi-

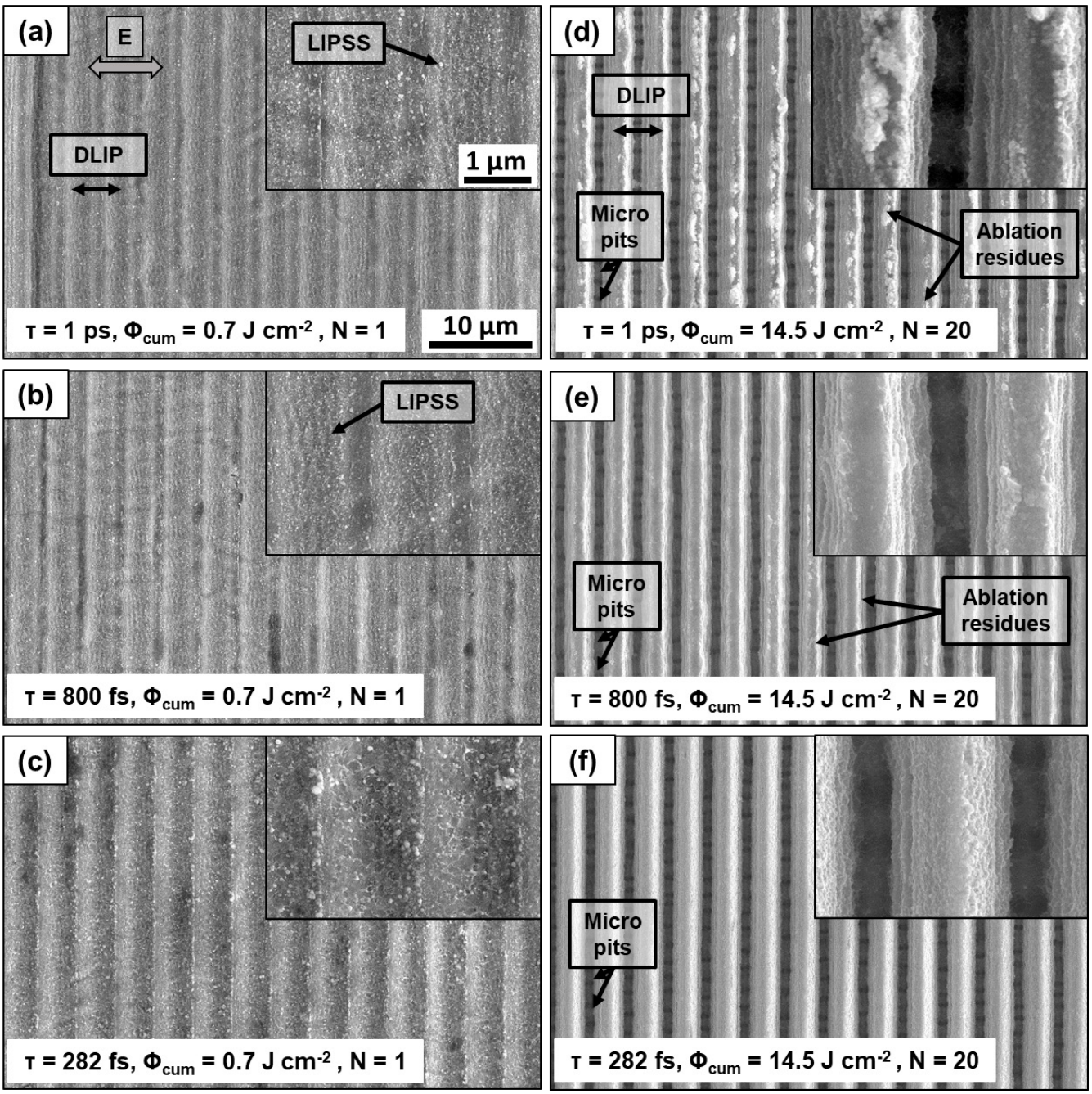

Fig. 2 SEM images of DLIP line-like structures produced on nickel-foils at a repetition rate frep = 1 kHz and overlap OV = 95%. The pulse duration, number of applied scans (N) and cumulated fluence (Φ_{cum}) are displayed in the corresponding labels.

ma positions becomes stronger, leading to deeper DLIP structures for all pulse durations as illustrated in Figure 2d, 2e and 2f. The appearance of self-organized periodic micro pits in the regions of the interference maxima and parallel to the DLIP lines could be also observed for all pulse durations. Furthermore, the micro pits exhibit a spatial distance of 1.5 ± 0.5 µm. From the SEM images (Figures 2d-f), it can be concluded that the formation of the micro pits was not influenced by the pulse duration and predominantly depended on the applied cumulated laser fluence. Furthermore, it is known that these features result from successive accumulation of the laser radiation (in particular when applying several laser pulses) as already explained by other authors [28]. In addition, the laser structuring experiments performed at 1 ps with 20 consecutive passes resulted in a surface with significant redeposition of ablated material on the ridges of the line-like features as illustrated in Figure 2d. Upon decreasing the pulse duration to 800 fs, the formation of ablation residues was significantly reduced (Figure 2e). For the sample treated with a pulse duration of 282 fs, the produced topography is free of residues. This can be explained due to the very rapid formation of vapor and plasma phases, with negligible heat conduction as well as the absence of a liquid phase for the femtosecond regime. It is also noticeable that the LSFL ripples in the region of maxima interference visible for one scan, vanished as a result of the laser process with high cumulative fluences (for 20 passes). Interestingly, for the surfaces treated with several over scans, fringes located in the walls of the produced lines are also visible. These features could result from interference effects between the incoming and reflected radiation, and are known as Newton fringes [29].

By confocal microscopy analysis, the dependence of the structure depth as a function of the cumulated laser fluence and the number of passes N was characterized. The results are summarized in Figure 3. The measured structure depths for the samples treated with a single scan (N = 1), using a pulse overlap of 95% and pulse fluence values between 0.02 and 0.04 J cm^{-2} are displayed in Figure 3a. The depth of the line-like DLIP textures can be observed to increase in an almost linear manner with the cumulated fluence. This behavior has been observed for all pulse durations. For the shortest pulse duration of 282 fs, the deepest DLIP features were generated along the whole range of cumulated fluence values. The maximum fluence of 0.73 J cm^{-2} resulted in case of a pulse duration of 282 fs in a structure depth of 0.37 ± 0.03 µm, while for 800 fs, a structure depth of 0.26 µm ± 0.06 µm was obtained. In case of the 1 ps pulse duration, the structure depth was 0.17 ± 0.06 µm, being this value approximately the half of the depth reached 282 fs. It is known that when using shorter laser pulses (in particular with pulse durations shorter than 1 ps), a lower amount of energy per unit of area is required to initiate ablation at the material surface since the absorbed energy is mainly used for the ablative process with almost no thermalization of the remaining material [30]. This effect can enhance therefore the ablation rate, as already reported for different metals [31].

Interestingly, the error bars associated with the depth measurements for the Ni-surfaces structured with a pulse duration of 282 fs were smaller than those resulting from 1 ps and 800 fs pulse durations. This indicates a higher overall texture homogeneity for the DLIP pattern produced in the low fs regime. A possible explanation could be due to the absence of ablation residues that are generated each time that the material surface is irradiated. In case of the longer pulses, these features might lead to inhomogeneities.

For the fabrication of DLIP line-like structures with high aspect ratios, the number of consecutive scans N was varied between 1 and 30. The measured structure depths as a function of the number of passes as well as the cumulative fluence values for the same pulse durations (282 fs, 800 fs and 1 ps) are shown in Figure 3b. As it can be seen, the depth increased continuously up to 20 consecutive scans, independently of the used pulse duration. For N = 20 passes and a cumulative fluence of 14.5 J cm^{-2}, maximal structure depths of 2.2 ± 0.19 µm, 1.5 ± 0.22 µm and 1.4 ± 0.25 µm where obtained for pulse durations of 282 fs,

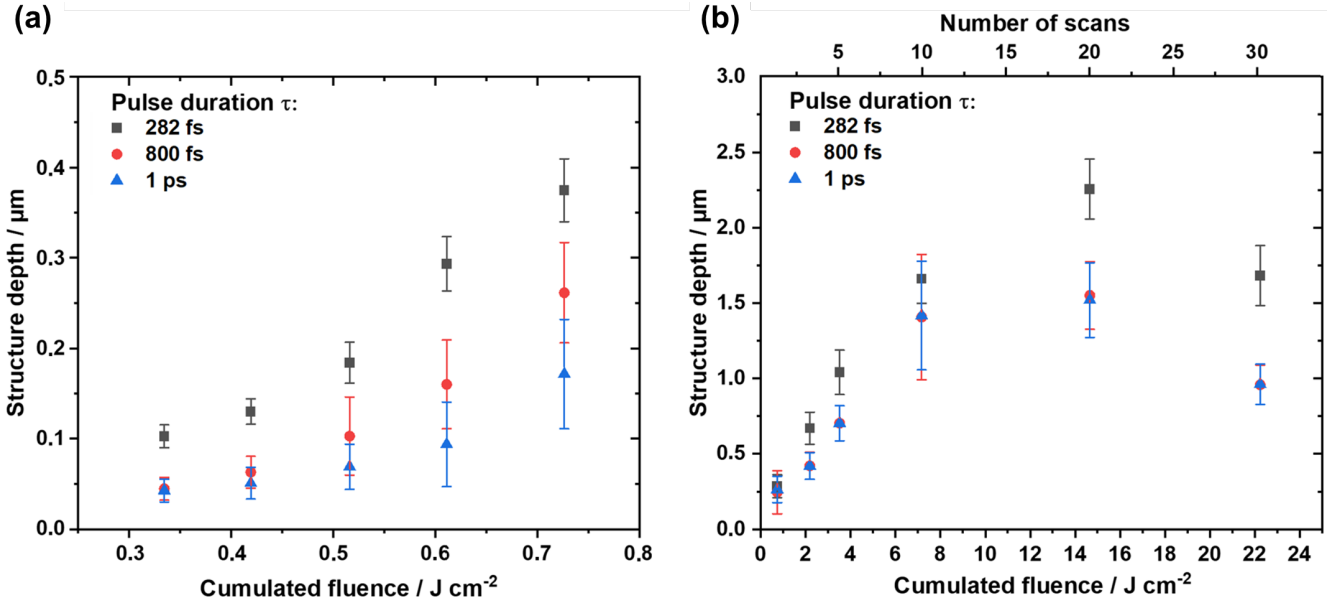

Fig. 3 Structure depth as function of the cumulated fluence for a) a single scan and b) multiple scans, using pulse durations of 282 fs, 1 ps and 10 ps.

800 fs and 1 ps, respectively. Clearly, since the samples are scanned several times, deeper structures can be obtained since a higher amount of material is ablated at the interference maxima positions. When the number of passes was increased further to 30, the structure depth decreased for all pulse durations. Although this behavior has been already reported in DLIP experiments performed with ns pulses, the reasons for this reduction in the structure depth is still unclear. It is possible that when periodic structured surfaces with a high aspect ratio (~ 0.6 to 0.8) are re-irradiated, this topography negatively affects the incoming pulse distorting the pattern. Further detailed investigations are necessary to answer this question.

Based on the information presented in the previous sections, larger Ni-electrodes with dimensions of 360 mm x 100 mm were processed, which were necessary for the hydrogen evolution reaction experiments. In addition to line-like patterns, also cross-like geometries were produced (also referred as pillar structures in the literature), by firstly producing line-like structures and subsequently rotating the samples by 90 ° and re-irradiating them. The reason for producing the cross-like geometries lies in a further enhancement of the surface area that can have a beneficial effect on the electrodes performance. In addition, since the deeper features were obtained for a pulse duration of 282 fs and 20 consecutive scans, only these process parameters were implemented. The electrodes produced exhibit a material throughput of 0.05 m²/min and 0.025 m²/min for the line and cross-like DLIP structures, respectively.

SEM images of the resulting textured samples together with the two-dimensional Fast Fourier Transform (2D-FFT) of the line and cross-like DLIP features are shown in Figure 4. The SEM images (Figure 4a and 4b) displayed highly uniform periodic surface features for both texture types. The corresponding FTT spectra for the line- and cross-like pattern is pictured in Figure 4c and d, respectively, showing the periodic distribution of clearly defined intensity peaks with an equidistant spacing, resembling the spectrum of perfectly ordered 1D and 2D diffraction gratings, respectively [32,33]. By measuring the distance between two adjacent intensity peaks, the spatial periods of the DLIP structures can be calculated, yielding a spatial period Λ of 3.0 µm for both texture types.

3.2 Determination of electrochemically active surface area

Previous studies have shown that the enlargement of the nickel electrode surface area is beneficial for the electrocatalytic HER activity [8,9,11]. The electrochemically active surface area (ECSA) plays a crucial role in determining the HER activity as it represents the interface area between the electrolyte and electrode, where the charge transfer reaction occurs. Electrochemically, the active surface could be estimated by measuring the double-layer capacitance C_{dl} [34]. Additionally, the enlargement of the ESCA compared to flat nickel electrodes can be quantified by

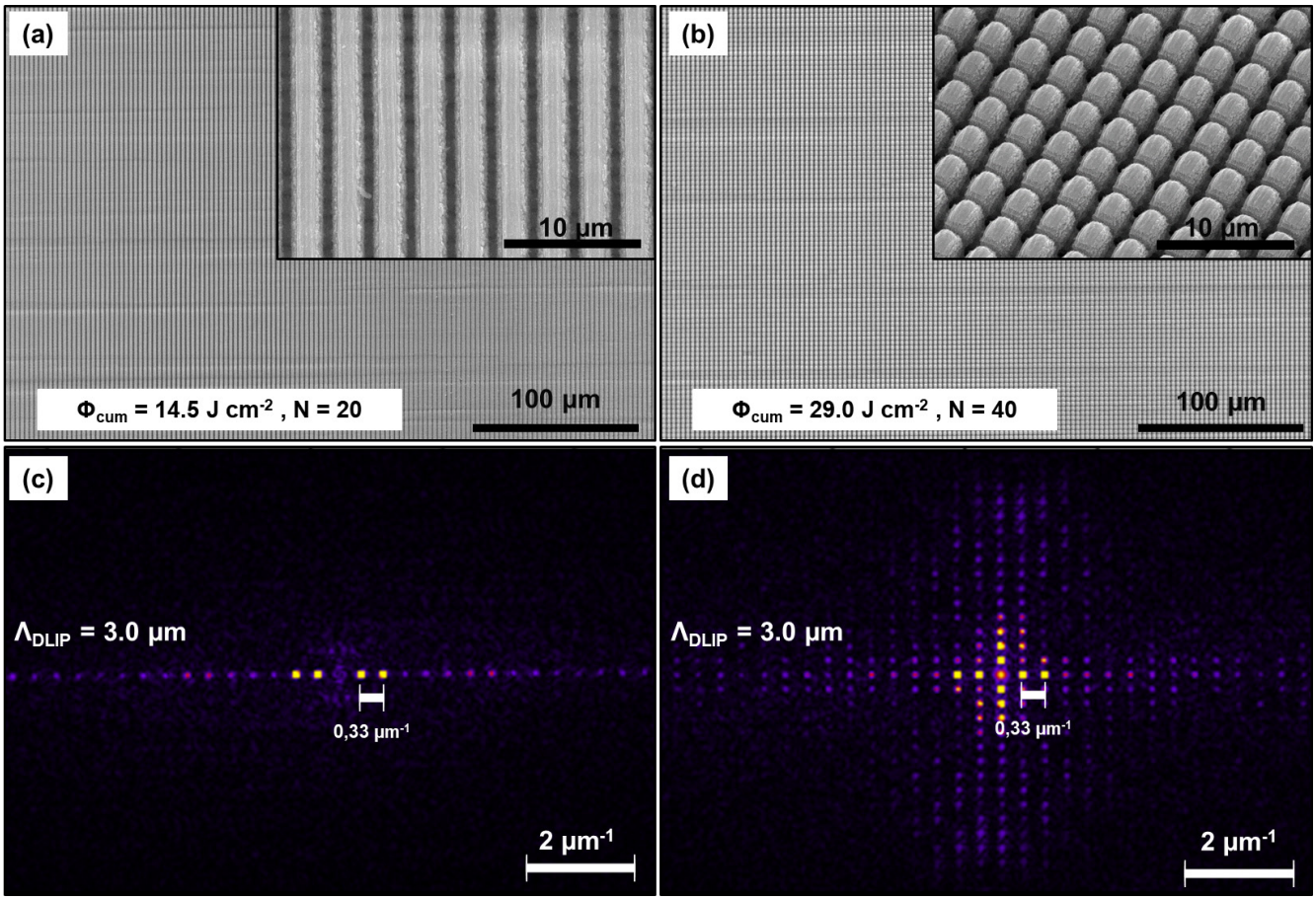

Fig. 4 SEM images of DLIP line-like (a) and cross-like (b) structures produced on nickel-foils at a pulse duration τ = 282 fs, repetition rate f_{rep} = 1 kHz, overlap OV = 95 % and hatch distance HD = 139 µm. The cumulated fluence (Φ_{cum}) and the total number of applied scans (N) are displayed in the corresponding labels. Two-dimensional Fast Fourier Transform for line-like (c) and cross-like (d) DLIP structure.

Table 1 Estimated double-layer capacitance C_{dl} at $|\eta_{HER}|$=100 mV after 1h at -0.5 A cm^{-2} in a 30wt.-%. KOH at 60 °C. Calculated roughness parameter R_f based on the capacitance values obtained from EIS. Overpotential $|\eta_{HER}|$ at a geometric current density of -0.5 A cm ². Tafel slope parameter $|b|$ and exchange current density j_0. Charge transfer resistance R_{ct} at $|\eta_{HER}|$ = 100 mV after 1h of the HER at -0.5 A cm^{-2}.

Ni-electrodes	Double-layer capacitance C_{dl} / mF cm^{-2}	Roughness factor R_f / -	Overpotential $\|\eta_{HER}\|$ / mV	Tafel slope $\|b\|$ / mV dec^{-1}	Exchange current density $j_{o,geo}$ / mA cm^{-2}	Charge transfer resistance R_{ct} / Ω cm^{-2}
Untreated	0.5	1.0	464	145	0.2	20.7
DLIP (line-like)	1.7	3.4	295	114	1.3	4.3
DLIP (cross-like)	4.9	9.8	227	98	2.3	1.4

introducing the dimensionless roughness parameter R_f of the untreated and the line- and cross-like structures [35]. Note that the ECSA could be smaller compared to the real electrode area if, for instance, parts of the surface are physically obstructed by adherent gas bubbles, due to the electrode/gas interface [36,37]. The C_{dl} values determined by EIS and the corresponding calculated roughness factor R_f are summarized in Table 1. For untreated Ni-electrodes a C_{dl} value of 0.5 mF cm^{-2} was observed under these conditions. An increased C_{dl} value and, therefore, an enhanced roughness factor was obtained for the DLIP-structured line-like and cross-like textures (Table 1). In case of the DLIP line-like treated electrode, a R_f value of 3.4 was determined, whereas DLIP with cross-like textures provided the largest roughness factor of 9.8 which indicated an increase of the ECSA of almost ten times in comparison to untreated Ni-electrode.

3.3 Electro-catalytic activity towards HER

An evaluation of the electro-catalytic activity towards HER in an alkaline medium was conducted on the DLIP-treated electrodes with line and cross-like geometries. The obtained results are shown in Figure 5. The overpotential-time curves for the laser textured specimens and the untreated Ni-electrode were recorded at a geometric current density of -0.5 A cm^{-2} for 1 h (Figure 5a). All curves exhibited an increasing overpotential over time, whereas the slope of the curve tended to slow down after the first 20 to 25 minutes. For the initial stages of HER, the overpotential gradually increased, which might be related to the reduction of native oxides or hydroxides and/or the formation of a thin nickel hydride layer consisting of a few atomic layers. After analyzing the curves depicted in Figure 5a, it could be concluded that treating the electrodes with fs-DLIP caused a translation of the overpotential-time curves towards lower overpotential values, relative to the untreated Ni-electrode. The resulting overpotentials after 1h of HER are listed in Table. 1.

The untreated nickel surface exhibited an overpotential of 464 mV, which aligns with results from previous studies [6,7]. In comparison, the DLIP (line-like) electrode displayed an overpotential of 295 mV, while the DLIP (cross-like) notably exhibited the lowest voltage overpotential value of 227 mV. In contrast to the untreated Ni-electrode, DLIP (cross-like) surface topography led to a significant decrease in overpotential by approximately 51 % and, consequently, led to higher reaction speeds towards HER.

To underpin the results for the HER activity, the kinetic behavior of HER was assessed by analyzing the steady-state polarization curves shown in Figure 5b. The corresponding Tafel parameters (b, j_0) for the tested electrodes are listed also in Table 1. Generally, the steady-state polari-

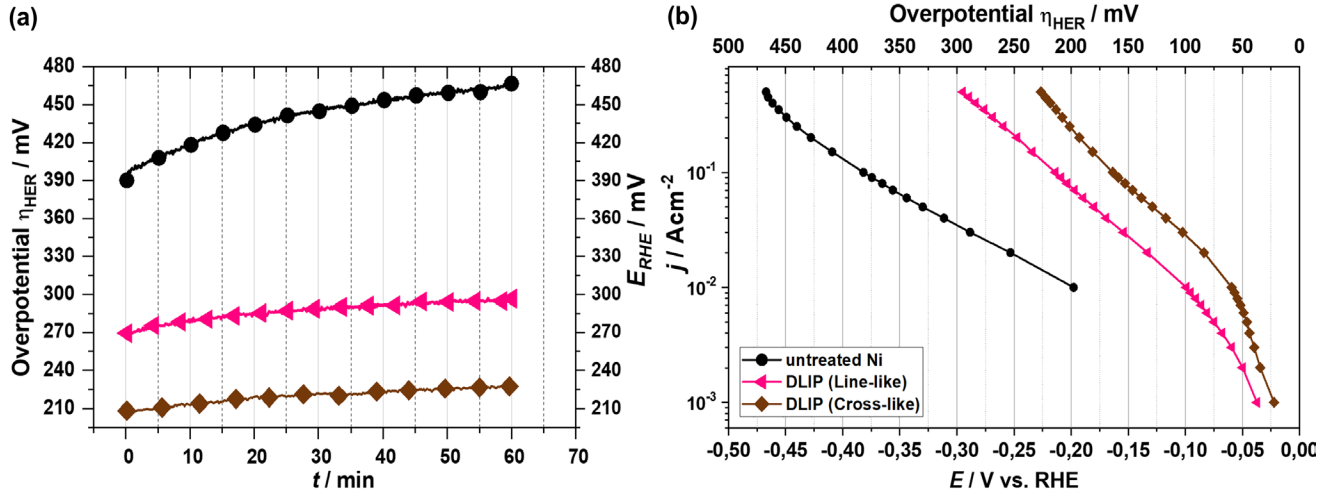

Fig. 5 (a) Overpotential-time curve of the hydrogen evolution reaction on the line and cross-like patterned Ni-electrodes compared to the untreated reference at a geometric current density of -0.5 A cm ² in 30 wt.% KOH at 60 °C for 1 h. (b) Steady-state polarization curves for untreated and line and cross-like DLIP structured Ni-electrodes.

zation curve reflected the HER activity presented in the overpotential-time curve. In this context, the untreated Ni-electrode exhibited the highest Tafel slope b (145 mV dec^{-1}) and the lowest exchange current density j_0 (0.3 mA cm^{-2}), indicating the lowest HER performance. In contrary, DLIP-treated the electrode (cross-like) showed the highest HER activity, coupled with the lowest Tafel slope parameter b (98 mV dec^{-1}), as well as the highest exchange current density j_0 (2.3 mA cm^{-2}). Generally, the activity towards HER is mainly influenced by the intrinsic activity and the electrochemically active surface area [35,38]. Therefore, it was further investigated whether the increase in ECSA is solely responsible for the reduction of the overpotential or if additional intrinsic effects influence the HER activity. In this context, the roughness factor R_f and the charge transfer resistances R_{ct} from the electrochemical impedance spectroscopy were further analyzed to examine the influence on the HER activity. The results are shown in Table 1. The DLIP microstructured electrode (cross-like) presented the highest roughness R_f value coupled with the lowest overpotential ($|\eta_{HER}|$= 227 mV), indicating that a larger electrochemical active surface area is accessible to the HER. This statement coincides with the SEM images displaying the periodic microstructure of the electrode. When comparing the roughness parameters (R_f) in relation to the overpotential ($|\eta_{HER}|$), it was observed that the DLIP (line-like) electrode exhibited an increase in ECSA by a factor of 3.4 (R_f= 3.4) and a reduction in overpotential by 36% compared to the untreated reference. In contrast, the periodic cross-like structure resulted in an almost tenfold increase (R_f = 9.8) in ECSA and a reduction in overpotential by approximately 51 % (as mentioned before). The non-proportional behavior regarding the surface enlargement coupled with the overpotential drop indicated that the intrinsic properties were influenced by the laser treatment.

The change in intrinsic activity of each electrode can be qualitatively assessed through the transfer charge resistances (R_{ct}). In this context, low R_{ct} values indicate high intrinsic activity. The results of R_{ct} are also indicated in Table 1. The untreated Ni-electrode exhibited an R_{ct} of 20.7 Ω cm^{-2} implying a low intrinsic activity. Whereby, for the laser-treated electrodes with line-like and cross-like textures lower R_{ct} values of 4.3 Ω cm^{-2} and 1.4 Ω cm^{-2} were observed, revealing that the enhanced HER activity for both electrodes was the result of the enlarged electrochemically active electrode surface area combined with a higher intrinsic activity.

4. Conclusion

In this work Direct Laser Interference Patterning (DLIP) was used to functionalize the nickel-based electrode surfaces with periodic microstructures. A pulsed laser source (ʎ = 514 nm) with tunable pulse duration between 282 fs and 1 ps, combined with a two-beam DLIP setup, was used to generate surface patterns with spatial periods of 3.0 µm and structure depths of up to ~ 2.8 µm. Both the pulse duration and number of applied scans were varied to assess the influence on the structure formation for line-like DLIP features. It was found that line-like patterns fabricated with a pulse duration 282 fs and N = 20 resulted in highly uniform periodic surface features with sharp well-defined textures and no traces of attached ablation residuals. In case of longer pulses (800 fs and 1 ps), the maximal structure depths decreased to ~ 1.5 µm (~ 42 % less compared to the patterns produced at 282 fs). In addition, a further increase of the scan numbers (from 20 to 30) resulted in narrower structures, probably due to distortions of the interference pattern during the texturing process. The determining factor for the achievable aspect ratio is predominantly the quantity of energy reaching the trench's bottom, which consequently facilitates material removal. Finally, Ni-electrodes with line and cross-like structures were fabricated and evaluated for hydrogen evolution reaction (HER). The results indicated that the DLIP-treated electrodes benefited from enlarged electrochemical active surface area and enhanced intrinsic activity which led to a considerable decrease of the overpotential of up to 51 % compared to the untreated Ni-electrode. These findings indicate that DLIP combined with femtosecond laser source can be employed to fabricate Ni electrodes at industrial scale for highly efficient production of hydrogen.

Acknowledgments

This project was funded by the European Regional Development Fund (ERDF) and co-financed under taxation on the basis of the budget adopted by the members of the Saxon State Parliament. Provision of the laser beam source by TOPAG Lasertechnik GmbH.

References

[1] K. Mazloomi and C. Gomes: Renew. Sustain. Energy Rev., 16, (2012) 3024.
[2] L. Fan, Z. Tu, and S.H. Chan: Energy Rep., 7, (2021) 8421.
[3] A. Gabler, C.I. Müller, T. Rauscher, M. Köhring, B. Kieback, L. Röntzsch, and W. Schade: Int. J. Hydrog. Energy, 42, (2017) 10826.
[4] V. Hoffmann, L. Hoffmann, W. Schade, T. Turek, and T. Gimpel: Int. J. Hydrog. Energy, 47, (2022) 20729.
[5] M. Koj, T. Gimpel, W. Schade, and T. Turek: Int. J. Hydrog. Energy, 44, (2019) 12671.
[6] T. Rauscher, C. I. Müller, A. Gabler, T. Gimpel, M. Köhring, B. Kieback, W. Schade, and L. Röntzsch: Electrochimica Acta, 247, (2017) 1130.
[7] C.I. Bernäcker, T. Gimpel, A. Bomm, T. Rauscher, S. Mauermann, M. Li, E.G. Hübner, W. Schade, and L. Röntzsch: J. Power Sources, 538, (2022) 231572.
[8] C.I. Bernäcker, T. Rauscher, T. Büttner, B. Kieback, and L. Röntzsch: J. Electrochem. Soc., 166, (2019) F357.
[9] W.J.F. Gannon and C.W. Dunnill: Electrochimica Acta, 322, (2019) 134687.
[10] D.S. Hall, C. Bock, and B.R. MacDougall: J. Electrochem. Soc., 160, (2013) F235.
[11] K. Lange, C. Hördemann, M. Schulz-Ruhtenberg, and J. Caro: ChemElectroChem, 5, (2018) 3688.
[12] N.K. Chaudhari, H. Jin, B. Kim, and K. Lee: Nanoscale, 9, (2017) 12231.
[13] S. Ahmad, M. Egilmez, A.M. Kannan, and A.S. Alnaser: Int. J. Hydrog. Energy, Part D, (2024).
[14] J. Park, S. Hyeon, S. Jeong, and H.-J. Kim: J. Ind. Eng. Chem., 70, (2019) 178.
[15] A.Y. Vorobyev and C. Guo: Laser Photon. Rev., 7, (2013) 385.

[16] J.A. Wahab, M.J. Ghazali, W.M.W. Yusoff, and Z. Sajuri: Int. J. Surf. Sci. Eng., 94, (2016) 193.
[17] C.I. Bernäcker, T. Gimpel, A. Bomm, T. Rauscher, S. Mauermann, M. Li, E.G. Hübner, W. Schade, and L. Röntzsch: J. Power Sources, 538, (2022) 231572.
[18] A.F. Lasagni, C. Gachot, K.E. Trinh, M. Hans, A. Rosenkranz, T. Roch, S. Eckhardt, T. Kunze, M. Bieda, D. Günther, V. Lang, and F. Mücklich: Proc. SPIE, Vol. 9351, (2017) 935115.
[19] F. Schell, S. Alamri, A. Hariharan, A. Gebert, A.F. Lasagni, and T. Kunze: Mater. Lett., 306, (2022) 130920.
[20] D.W. Müller, T. Fox, P.G. Grützmacher, S. Suarez, and F. Mücklich: Sci. Rep., 10, (2020) 3647.
[21]R. Baumann, T. Rauscher, C.I. Bernäcker, C. Zwahr, T. Weißgärber, L. Röntzsch, and A.F. Lasagni: J. Laser Micro Nanoeigin., 15, (2020) 2.
[22] A.F. Lasagni and B. Voisiat: Patent DE102020204656A1 (2021).
[23] E.B. Castro, M.J. de Giz, E.R. Gonzaleza, and J.R. Vilche: Electrochimica Acta, 42, (1997) 951.
[24] J. Bonse, M. Munz, and H. Sturm: J. Appl. Phys., 97, (2005) 013538.
[25] J. Bonse, S. Höhm, S.V. Kirner, A. Rosenfeld, and J. Krüger: IEEE J. Sel. Top. Quantum Electron., 23 (2017) 3.
[26] J. Bonse, J. Krüger, S. Höhm, and A. Rosenfeld: J. Laser Appl., 24, (2012) 042006.
[27] J. Bonse and S. Gräf: Laser Photonics Rev., 14, (2020) 2000215.
[28]E.J.Y. Ling, J. Saïd, N. Brodusch, R. Gauvin, P. Servio, and A.-M. Kietzig: Appl. Surf. Sci., 353, (2015) 512.
[29] T.-H. Lin, Y.-K. Yang, and C.-C. Fu: Nanotechnology, 28, (2017) 475301.
[30] B.C. Stuart, M.D. Feit, S. Herman, A.M. Rubenchik, B.W. Shore, and M.D. Perry: J. Opt. Soc. Am. B 1, 13, (1996) 459.
[31] J. Winter, M. Spellauge, J. Hermann, C. Eulenkamp, H. P. Huber, and M. Schmidt: Opt. Express, 29, (2021) 14561.
[32] N. Schröder, C. Fischer, M. Soldera, B. Voisiat, and A.F. Lasagni: Adv. Eng. Mater., 25, (2023) 2201889.
[33] N. Schröder, C. Fischer, M. Soldera, F. Bouchard, B. Voisiat, and A.F. Lasagni: Mater. Lett., 324, (2022) 132794.
[34] R. De Levie: Electrochimica Acta, 10, (1965) 395.
[35] I. Herraiz-Cardona, E. Ortega, J.G. Antón, and V. Pérez-Herranz: Int. J. Hydrog. Energy, 36, (2011) 9428.
[36] J. Eigeldinger and H. Vogt: Electrochimica Acta, 45, (2000) 4449.
[37] H. Vogt and R.J. Balzer: Electrochimica Acta, 50, (2005) 2073.
[38] C. González-Buch, I. Herraiz-Cardona, E. Ortega, J. García-Antón, and V. Pérez-Herranz: J. Appl. Electrochem., 46, (2016) 791.

(Received: August 23, 2023, Accepted: March 29, 2024)